splittings alone were chosen in order to be compatible with the ab initio results[5] and with model calculations from bond moments.

Discussion

In Table IV the microwave gas-phase structure of glycolic acid is compared with the crystal structure from neutron diffraction determined by Ellison et al.[1]

Similar results were obtained by Pijper except that the positions of the hydrogen nuclei were less accurately determined from the X-ray diffraction.[2] Relatively large differences in the bond lengths of typically 0.02–0.03 Å in the bond angles up to 4.5° are observed between the gas-phase and solid-state structures. The differences may be traced back to extensive changes in the hydrogen bonding, i.e., intramolecular in the gas phase and intermolecular in the solid state. The skeleton of the heavy nuclei is still nearly planar in the crystal, but the torsion angle τ ($C_1C_2O_5H_8$) of the alcoholic hydroxyl group changes from 0° to −80° while forming one of the intermolecular hydrogen bonds. In the crystal, molecules are linked via strong short hydrogen bonds O_3–H_9···O_5' of 1.64 Å and O_5–H_8···O_4'' of 1.76 Å. Apparently, this strong hydrogen bonding compensates for the deformations from the geometry of free glycolic acid, i.e., the breakage of the relatively weak intramolecular hydrogen bond O_5–H_8···O_4 of 2.11 Å, the strain energy in the hydroxyl torsion, and the remaining deformations of the bond lengths and bond angles.

Acknowledgment. Financial support by the Swiss National Foundation (Project No. 2.612–0.80) is gratefully acknowledged. We thank N. Schwizgebel and G. Grassi for the preparation of isotopic species and Dr. H. Hollenstein for helpful discussions.

Registry No. $CH_2OHCOOH$, 79-14-1; $CH_2OH^{13}COOH$, 81277-96-5; $^{13}CH_2OHCOOH$, 81277-97-6; $CH_2OHCO^{18}OH$, 81277-98-7; $CH_2OHC^{18}OOH$, 81456-63-5; $CH_2{}^{18}OHCOOH$, 81277-99-8; CHDOHCOOH, 73654-45-2; $CH_2ODCOOH$, 81278-00-4; $CH_2OHCOOD$, 81278-01-5; $CH_2ODCOOD$, 81278-02-6.

Supplementary Material Available: Listings of measured rotational transition frequencies of CHDOHCOOH, $CH_2OH^{13}COOH$, $^{13}CH_2OHCOOH$, $CH_2OHCO^{18}OH$, $CH_2OHC^{18}OOH$, $CH_2{}^{18}OHCOOH$, $CH_2ODCOOH$, $CH_2OHCOOD$, and $CH_2ODCOOD$ in the vibrational ground state and least-squares fits of moments of inertia and shifts for glycolic acid and nine isotopic substituted species (Tables V–VII) (5 pages). Ordering information is given on any current masthead page.

Visible Light Induced Water Cleavage in Colloidal Solutions of Chromium-Doped Titanium Dioxide Particles[1a]

Enrico Borgarello,[1b] John Kiwi,[1b] Michael Grätzel,*[1b] Ezio Pelizzetti,[1c] and Mario Visca[1d]

Contribution from the Institut de Chimie Physique, Ecole Polytechnique Fédérale, CH-1015 Lausanne, Switzerland, the Istituto di Chimica Analitica, Università di Torino, Italy, and the Centro Richerche SIBIT, Spinetta Marengo, Italy. *Received October 13, 1981*

Abstract: Surface doping of colloidal TiO_2 particles with chromic ions precipitated from aqueous H_2SO_4 solution produces very small (<0.1 μm) mixed-oxide particles which absorb light in the 400–550-nm region in addition to the band-gap absorption of anatase. Sustained water cleavage by visible light is observed in aqueous solutions of these particles. Ultrafine deposits of Pt or RuO_2 are necessary to promote water decomposition. A pronounced synergistic effect in catalytic activity is noted when both RuO_2 and Pt are codeposited onto the particle. Wavelength dependency and kinetics of H_2 and O_2 evolution are examined.

Impurity doping is an important technique for improving the response of TiO_2-based photoelectrolysis cells.[2-8] While some dopants such as Be or Al ions increase the minority carrier diffusion length,[4] others such as Cr,[2,3,5b,6,8,9] Cd,[4c] or Co[5a] ions extend the spectral response of TiO_2 into the visible by inducing optical transitions from d electrons of the metal to the TiO_2 (or $SrTiO_3$) conduction band. Chromium ions substituted for Ti^{4+} in the TiO_2 lattice have so far yielded optimal results. However, the Cr centers in TiO_2 have a low oscillator strength ($\sim 10^{-4}$) which in view of the low solubility of Cr in this oxide (0.4 a/o) renders visible light harvesting by these electrodes inefficient. Moveover, Cr affects adversely the photocurrent in the band-gap region of TiO_2 due to a decrease in the hole diffusion length. At least for polycrystalline electrodes, this effect overcompensates the gain in overall conversion efficiency, which would be expected from the extension of the photoresponse towards the visible part of the spectrum.[4c]

In connection with our ongoing research on combined catalytic systems affording water cleavage by visible light,[10-17] we have performed extensive investigations with TiO_2 particles loaded with ultrafine deposits of Pt and RuO_2.[11-15,17] During these experiments, it was discovered that direct band-gap excitation of the TiO_2 sol

(1) (a) Presented in part at the Solar World Forum, Brighton, England, August 1981. (b) Institut de Chimie Physique. (c) Instituto di Chimica Analitica. (d) Centro Richerche SIBIT.

(2) Ghosh, A. K.; Maruska, H. P. *J. Electrochem. Soc.* **1977**, *124*, 1516.
(3) Maruska, H. P.; Ghosh, A. K. *Sol. Energy Mater.* **1979**, *1*, 237.
(4) (a) Augustynski, J.; Hinden, J.; Stalder, C. *J. Electrochem. Soc.* **1977**, *124*, 1063. (b) Stalder, C.; Augustynski, J. *Ibid.* **1979**, *126*, 2007. (c) Monnier, A.; Augustynski, J. *Ibid.* **1980**, *127*, 1576.
(5) (a) Matsumoto, Y.; Kurimoto, J.; Amagasaki, Y.; Sato, E. *J. Electrochem. Soc.* **1980**, *127*, 2148. (b) Matsumoto, Y.; Kurimoto, J.; Shimizu, T.; Sato, E. *Ibid.* **1981**, *128*, 1040.
(6) Lampet, G.; Verniolle, J.; Doumere, J. P.; Claverie, J. *Mater. Res. Bull*, **1980**, *15*, 115.
(7) Goodenough, J. B. *Prog. Solid State Chem.* **1971**, *5*, 145–344.
(8) Mackor, A.; Blasse, G. *Chem. Phys. Lett.* **1981**, *77*, 6.
(9) Houlihan, J. F.; Armitage, D. B.; Hoovler, T.; Bonaquist, D.; Madacsi, D. P.; Mulay, L. N. *Mater. Res. Bull.* **1978**, *13*, 1205.
(10) Kalyanasundaram, K.; Grätzel, M. *Angew. Chem., Int. Ed. Engl.* **1979**, *18*, 701.
(11) Kiwi, J.; Borgarello, E.; Pelizzetti, E.; Visca, M.; Grätzel, M. *Angew. Chem., Int. Ed. Engl.* **1980**, *19*, 646.
(12) Grätzel, M. *Ber. Bunsenges. Phys. Chem.* **1980**, *84*, 981.
(13) Borgarello, E.; Kiwi, J.; Pelizzetti, E.; Visca, M.; Grätzel, M. *Nature (London)* **1981**, *284*, 158; *J. Am. Chem. Soc.* **1981**, *103*, 6423.
(14) Kalyanasundaram, K.; Grätzel, M. NATO Advanced Studies Treatise, NATO Summer School on Photoelectrochemistry, Gent, Belgium, 1980.
(15) Kalyanasundaram, K.; Borgarello, E.; Grätzel, M. *Helv. Chim. Acta* **1981**, *64*, 362.
(16) Duonghong, D.; Borgarello, E.; Grätzel, M. *J. Am. Chem. Soc.* **1981**, *103*, 4685.
(17) Grätzel, M. *Faraday Discuss. Chem. Soc.* **1980**, *70*, 359.

0002-7863/82/1504-2996$01.25/0

produces oxygen and hydrogen at a high quantum yield. In order to shift the onset wavelength required for water cleavage into the visible, it appeared tempting to apply the concept of transition-metal doping to our TiO_2 particles. This has the attractive feature that the dimensions of colloidal semiconductors are small enough to render excape of photoinduced holes to the particle surface efficient even if the diffusion lengths were intolerably short for electrode devices. Small extinction coefficients in the visible are also not problematic since they can be compensated for by using higher colloid concentrations. The success of such a strategy is documented by the water-cleavage experiments described below.

Experimental Section

Materials. Hexachloroplatinic acid was a kind gift from Engelhard Industries. All other compounds were at least reagent grade and used as supplied. Deionized water was distilled from alkaline $KMnO_4$ and subsequently distilled twice from a quartz still.

Catalyst Preparation. TiO_2 (anatase) was prepared by thermal hydrolysis of titanium sulfate according to the Blumenfeld procedure.[18] Upon dilution a gellike material is precipitated. To this slurry was added the calculated amount of $K_2Cr_2O_7$ (570–2860 μg of Cr/g of TiO_2). The products were thoroughly mixed, filtered, and subsequently annealed at 400 °C for 1 h. In some cases the heat treatment was performed at 750 °C.

Loading with RuO_2 was carried out by dispersing the Cr-doped TiO_2 particles in a concentrated aqueous solution containing 3 mg of $RuCl_3$/g of TiO_2 (this corresponds to 0.2% loading with RuO_2). After adjustment of the pH to 6 with KOH, the product was filtered and dried overnight at 100 °C.

Loading with Pt was always performed as the last step in the catalyst preparation. At first a solution of H_2PtCl_6 was refluxed with citrate in a separate container. It is of vital importance for the successful preparation of highly active catalysts to maintain the temperature during the reduction at 80–90 °C. After 3–4-h reaction time, one obtains a yellow Pt sol[13] consisting of Pt embryos with a mean diameter of 15 Å.[19] (These ultrafine Pt particles are inactive as catalysts for H_2O_2 decomposition.[20] Refluxing at 100 °C as previously described by Turkevich and others[19-23] yields 30-Å-sized particles, which catalyze efficiently H_2O_2 decomposition but are less suited for H_2 generation in cyclic water cleavage systems.) The ultrafine Pt sol is subsequently mixed with the solution containing the TiO_2/RuO_2 particles and sonicated in a water bath.[24] The loading of Pt employed is 10 mg of Pt/g of TiO_2, i.e., 1%.

Characterization of the Catalyst. Application of static and dynamic light scattering technique, in particular multiangle measurements for the determination of the radius of gyration,[25] reveals a prolate structure of the particles, the short and long axis being 1500 and 300 Å, respectively. The material itself consists mainly of amorphous oriented anatase (≥85%), as shown by X-ray analysis.

The surface area as determined by BET adsorption measurements is very high and amounts to 200–240 m^2/g.

Optical absorption spectra of doped and undoped TiO_2 powders were obtained by diffuse reflectance spectroscopy. Representative examples are given in Figure 1. Undoped TiO_2 loaded with RuO_2 exhibits no absorption in the visible. The small, barely noticeable hump around 450 nm arises from the $RuCl_3$ treatment of the TiO_2 particles. No photoactivity is associated with this extremely weak transition, as will be shown below. An absorption edge rising steeply toward the UV below 380 nm can be attributed to band-gap excitation of anatase (380 nm corresponds to 3.2 eV, which is identical with the optical band gap of anatase.)[26] Chromium doping introduces a band in the visible that starts below 550 nm and shows a maximum at 450 nm. This transtition can

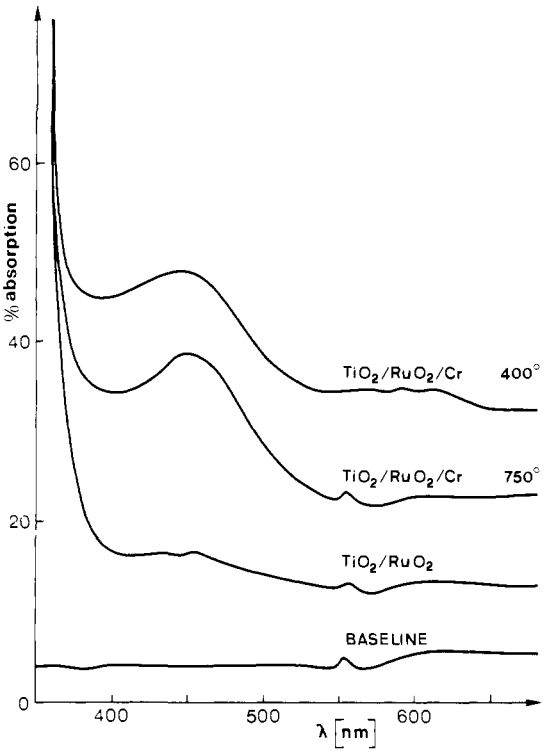

Figure 1. Visible and near-UV absorption spectrum of TiO_2/RuO_2 particles in the absence and presence of surface doping with chromic ions (570 ppm, w/w). Annealing for 1 h at 400 or 750 °C. Spectra measured by diffuse reflectance spectroscopy.

be attributed[27] to the $Cr^{3+} \rightarrow Ti^{4+}$ charge-transfer excitation or, in the semiconductor language, the excitation of an electron of Cr^{3+} into the conduction band of TiO_2.[28] Noteworthy in Figure 1 is also the fact that the band-gap absorption of TiO_2 is not affected by Cr doping. The band gap coincides precisely with that obtained from Cr-free samples. Furthermore, it appears that increasing the temperature of annealing from 400 to 750 °C enhances the visible absorption of the particles.

Apparatus and Evaluation of Water Cleavage Experiments. Continuous illuminations were carried out with an Osram XBO 450-W Xe lamp equipped with a 15-cm water jacket to remove IR radiation. For visible light experiments, a 415-nm cutoff filter was placed in the beam. The optical density of the filter is 0.5 at 415 nm and 3 at 401 nm, which suffices to suppress entirely any direct band-gap excitation of TiO_2. The total visible light intensity impinging on the simple cell corresponds to an energy flux of 500 mW/cm^2. The solution volume was invariably 25 mL and was contained in a Pyrex flask equipped with optically flat entry and exit windows. The transmission of the pyrex window is 50% at 325 nm and practically zero below 300 nm. (The gas volume above the solution is ca. 10 mL.)

The gas evloved under illumination was analyzed by gas chromatograpy. A GOW-MAC system, carbosieve column (35 °C), and N_2 as a carrier gas were employed for hydrogen detection. Oxygen was detected by using a Perkin-Elmer 900 GC with a 6 ft × 118 in. molecular sieve (5 Å) column. The carrier gas was He, and the column temperature was maintained at 40 °C. The filament was set at 225 mA (TCD mode) and attenuation 16.

An alternative way of oxygen detection consisted in using a Teledyne B_1 oxygen-specific microfuel cell. The electrode is placed in a small cylindrical glass vessel, which is connected through a flow system[16] with the sample cell. Prior to illumination the whole system is freed from oxygen by a stream of N_2. The solution is then exposed to light. The gas produced under illumination is transferred to the detector by the carrier gas. The N_2 flow through the solution is either continuous or is intercepted during illumination. In the latter case, the gas produced by the photolysis is sampled at regular intervals. By using this method, the time characteristic of O_2 generation could be established.

(18) "Titanium"; Barksdale, J., Ed.; Ronald Press: New York, 1966.
(19) Turkevich, J., private communication. Measurements of particle size were carried out with the Brookhaven National Laboratory electron microscope having a resolution of 3 Å.
(20) Turkevich, J.; Aika, K.; Ban, L. L.; Okura, I.; Namba, S. *J. Res. Inst. Catal., Hokkaido Univ.* **1976**, *24*, 54.
(21) Turkevich, J. In "Electrocatalysis of Fuel Cell Reactions", Brookhaven Symposium proceedings, 1978; p 123.
(22) Wilenziok, R. M.; Russell, D. C.; Morris, R. J.; Marshall, S. W. *J. Chem. Phys.* **1967**, *47*, 533.
(23) Brugger, P.-A.; Cuendet, P.; Grätzel, M. *J. Am. Chem. Soc.* **1981**, *103*, 4685.
(24) Further details about catalyst preparation and the removal of excess citrate have been given in ref 13.
(25) Corti, M.; Pelizzetti, E., to be published.
(26) Kruczynski, L.; Gesser, H. O.; Turner, C. W.; Speers, E. A. *Nature (London)* **1981**, *291*, 399.
(27) The 4 $A_2 \rightarrow 4$ T_2 metal-centered d^3 transition of Cr^{3+} is located at 650 nm. This transition is symmetry forbidden and hence very weak. See: Blasse, G. *J. Inorg. Nucl. Chem.* **1967**, *29*, 1817.
(28) Although Cr is added to the TiO_2 dispersion Cr_2O_7, i.e., in the oxidation state 6, oxygen loss and hence reduction to the 3^+ state occur during the thermally activated substitution for Ti^{4+} in the TiO_2 lattice.

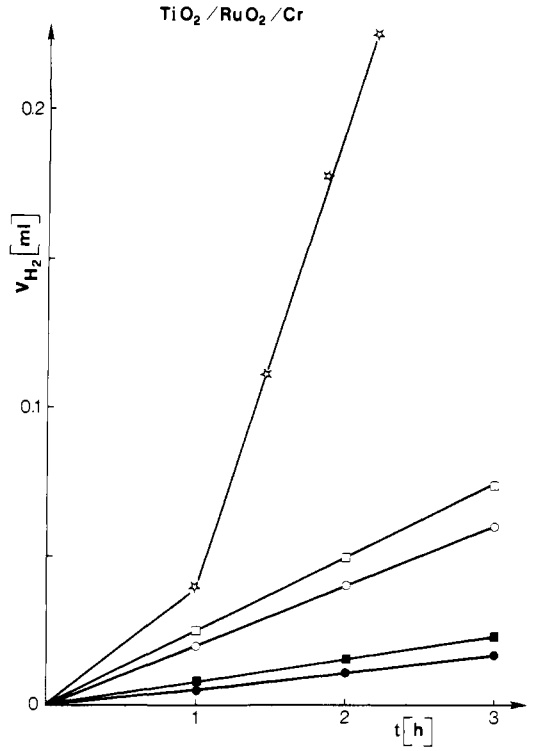

Figure 2. Visible light ($\lambda > 415$ nm) irradiation of $TiO_2/RuO_2/Cr$ dispersions in methanol (25 mg/25 mL). Volume of H_2 evolved is plotted against irradiation time. Conditions: (*) RuO_2 (0.2%), Cr^{3+} (570 ppm), annealing temperature 400 °C; (□) annealing temperature changed to 750 °C; (○) doping with Cr^{3+} increased to 1430 ppm, annealing temperature 400 °C; (■) no RuO_2, Cr^{3+} (570 ppm), annealing temperature 700 °C; (●) RuO_2 (0.2%), Cr^{3+} (2860 ppm), annealing temperature 400 °C.

Results

Optimization of Catalysts for Visible Light Induced Hydrogen Generation. The purpose of these experiments was to identify optimum conditions of catalyst preparation and composition for visible light induced hydrogen generation. The simultaneous formation of oxygen, which frequently complicates the analysis, was avoided by using sacrificial organic compounds (methanol and EDTA) as a source of electrons for the reduction process. In a first series of experiments, methanolic solutions of the catalyst (25 mg/25 mL) were exposed to visible light ($\lambda > 400$ nm), and the volume of H_2 produced was measured as a function of irradiation time. Representative data obtained with catalysts containing different amounts of dopant and annealed at different temperatures are shown in Figure 2. A first apparent trend is that the rate of hydrogen generation ($r(H_2)$) decreases drastically with increasing Cr content of the catalyst. Thus, samples of TiO_2/RuO_2 containing 570 ppm Cr^{3+} yield under stationary conditions $r(H_2) = 150$ μL/h, while those with 2860 ppm give only 4 μL/h. Next, we note that increasing the annealing temperature of the 570 ppm Cr catalyst during preparation from 400 to 700 °C decreases $r(H_2)$ by a factor of 6.

Finally, the loading with RuO_2 appears to be important as the omission of this catalyst decreases the hydrogen output by a factor of 2 in the case of TiO_2/Cr (570 ppm) annealed at 700 °C.

A second series of experiments was performed in aqueous solutions (pH 5) containing 10^{-2} M EDTA as an electron donor. Optimal results were again obtianed with the TiO_2 particles containing 570 ppm Cr^{3+} and annealed at 400 °C. Catalysts loaded with 0.2% RuO_2 gave a stationary H_2 generation rate of 60 μL/h. This rate could be improved to 400 μL/h by depositing 1% Pt in addition to RuO_2 onto the particles.

These observations may be explained in terms of excitation of electrons from Cr^{3+} centers to the conduction band of TiO_2 by visible light. These electrons subsequently reduce methanol or water to H_2. The holes migrate to the particle surface[29] where oxidation of methanol[30] to formaldehyde (or ultimately formic acid and CO_2) occurs. In aqueous EDTA solutions the holes are scavenged by EDTA, which is irreversibly oxidized according to a mechanism dealt with elsewhere.[31] The role of RuO_2 is to promote hole transfer from the valence band of the particle to the organic electron donor in solution while Pt catalyzes the reduction of water to hydrogen.

As for the effect of Cr^{3+} doping on $r(H_2)$, one expects from our mode of catalyst preparation that Cr^{3+} is present mainly in the surface region of the particles. Increasing the Cr^{3+} doping much beyond its solubility limit in TiO_2 (~0.4%) is likely to produce a chromic oxide surface layer that is photochemically inactive and that through its insulating and light-absorbing properties reduces the photoactivity of the TiO_2 particles. As to the adverse effect of high-temperature annealing on $r(H_2)$, we attribute this mainly to the drastic reduction in the surface area of the TiO_2 support caused by such a treatment.[32] This will affect also the structural organization of the Cr^{3+}-enriched surface layer of TiO_2 which will accommodate only a smaller number of dopant sites. In this context it is interesting to point out that for polycrystalline TiO_2 electrodes the optimal annealing temperature and Cr^{3+} doping level are ~500 °C and 0.4% (a/o), respectively,[4] which agrees well with the optimal conditions for our colloids.

Cyclic Water Cleavage Experiments. These experiments were performed in pure water (pH 3, adjusted with HCl) and strict attention was payed to the absence of any organic agent that could replace water as an electron source. Colloidal TiO_2 suspensions were illuminated with different wavelength domains of exciting light, and the amount of H_2 and O_2 evolved was measured as a function of irradiation time. All experiments were performed with 25-mL volume solutions in a closed cell, which prior to illumination was freed from oxygen by flushing with N_2. While under these conditions the appearance of H_2 in the gas phase is always prompt, that of O_2 is delayed due to adsorption onto the TiO_2 particles. Stoichiometric yields are obtained only after saturation of the surface sites. This effect has very important implications for the efficiency of light-induced water decomposition and will therefore be dealt with separately below. In the following we shall first concentrate on the kinetics of H_2 generation and investigate it as a function of catalyst composition and excitation wavelength.

In a series of preliminary tests, it was first established that also in the case of cyclic water cleavage the TiO_2/Cr (570 ppm) particles annealed at 400 °C performed best among the various catalysts tested before in the sacrificial systems. The results presented in the following refer therefore always to this type of chromium-doped TiO_2. Irradiation of these particles (25 mg/25 mL solution) with visible light produces hydrogen at a very small rate, i.e., ca. 1.5 μL/h. Apparently the presence of redox catalysts is required to enhance the water-splitting activity. Figure 3 refers to TiO_2/Cr catalysts loaded with 0.2% RuO_2. Rates of hydrogen generation are here 15 μL/h, 100 μL/h, and 350 μL/h when 415-, 360-, and 300-nm (Pyrex) cutoff filters are placed in the light beam, respectively. Upon renewed insertion of the 415-nm filter, H_2 generation resumes at the initial rate of 15 μL/h. A long-term irradiation showed that this rate can be sustained over at least 600 h, producing a total of 9 mL or 4×10^{-4}M H_2. Turnover numbers are 1300, 150, and 1.3 mol of H_2 per mol of RuO_2, Cr, and TiO_2 catalysts, respectively. In order to establish that visible light induced water decomposition arises from Cr^{3+} doping, we performed blank experiments with chromium-free TiO_2/RuO_2 dispersions. No hydrogen at all was generated if the 415-nm cutoff filter was placed in the light beam. In contrast, irradiation through the 360- and 300-nm filter gave practically the same H_2 yield as

(29) Hole migration has been suggested to occur via tunneling from Cr^{4+} to the TiO_2 valence band.

(30) For the mechanism of methanol oxidation by valence band holes of TiO_2, compare, e.g.; Kawai, T.; Sakata, T. *J. Chem. Soc., Chem. Commun.* **1980**, 694.

(31) For oxidation of EDTA on semiconductor powders, see: (a) Darwent, J. R.; Porter, G. *J. Chem. Soc., Chem. Commun.* **1981**, 145. (b) Kalyanasundaram, K.; Borgarello, E.; Grätzel, M. *Helv. Chim. Acta* **1981**, *64*, 362. Harbour, J. R.; Hair, M. L. *J. Phys. Chem.* **1977**, *81*, 1791.

(32) Parfitt, D. G. *Prog. Surf. Membr. Sci.* **1976**, *11*, 181.

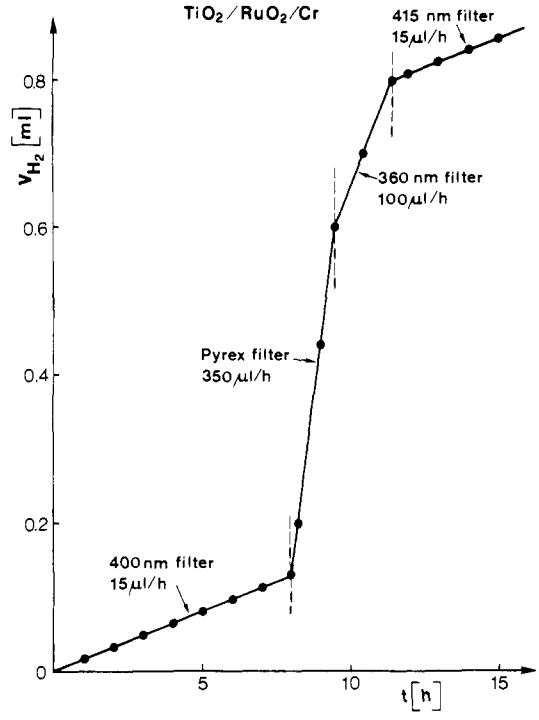

Figure 3. Light-induced water cleavage in TiO_2/Cr dispersions (Cr doping 570 ppm, annealed at 400 °C), loaded with 0.2% RuO_2. Volume of H_2 produced as a function of irradiation time. Filters used are indicated.

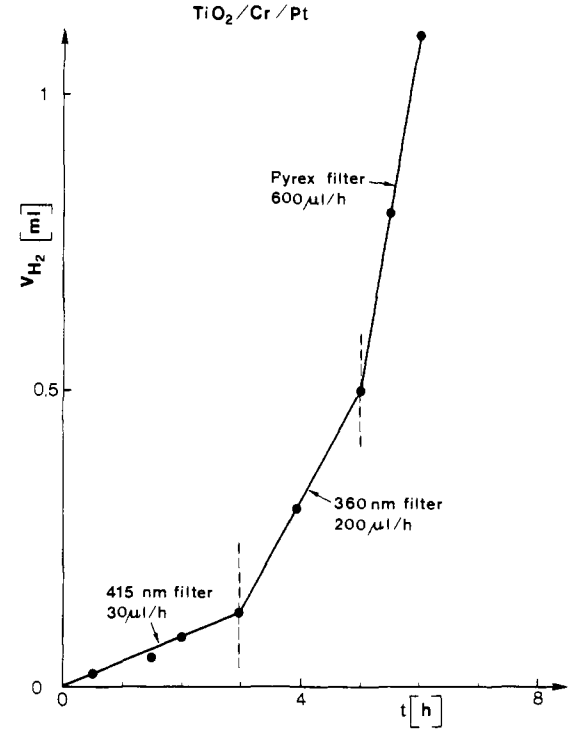

Figure 4. Light-induced water cleavage in TiO_2/Cr dispersions (Cr doping 570 ppm, annealed at 400 °C) loaded with 1% Pt. Volume of H_2 produced as a function of irradiation time. Filters used are indicated.

obtained with the chromium-doped TiO_2/RuO_2 particles.

Irradiation experiments were carried out also with TiO_2/Cr colloids that were loaded with Pt instead of RuO_2 as a redox catalyst. Results are presented in Figure 4. The hydrogen generation proceeds here at rates of 30, 200, and 600 μL/h for excitation with light of wavelengths greater than 400, 360, and 300 nm, respectively. Again, blank experiments with undoped TiO_2 particles showed that no H_2 was produced with visible light (415-nm cutoff), while under irradiation with UV light about the same amount of H_2 was generated as with the Cr-doped catalyst.

Figure 5 illustrates the catalytic activity of TiO_2/Cr particles loaded with both Pt and RuO_2 (bifunctional redox catalyst). Illumination commenced with the 400-nm cutoff filter inserted in the light beam. Visible light induced water decomposition proceeds at a rate of 200 μL of H_2/h. Exchange of the 415- against a 360-nm cutoff filter increases $r(H_2)$ to 600 μL/h. A further enhancement of the rate of 1.2 mL of H_2/h is observed when the filter is removed and the wavelength of incoming light is restricted to $\lambda > 300$ nm by the transmission properties of the Pyrex window of the flask. Figure 5 depicts also the behavior of the system when the light is turned off and the solution is kept in the dark. Recombination of H_2 and O_2 was observed, the initial rate for this reaction being around 0.8 mL/h. After completion of the recombination and deaeration of the solution with N_2, light-induced water cleavage resumes at the initial rate. This cycle can be repeated many times. We noted nevertheless that if illumination in a closed system is not interrupted, a photostationary state will eventually be reached where H_2 generation and recombination occur at the same rate. One would expect that the time required to reach that state should depend on the rate with which H_2 is generated. Data in Figure 5 include an overnight run with visible light. A total of 1.3 mL of H_2 was produced during 8 h, corresponding to an average rate of 163 μL of H_2/h. This is only 20% smaller than the $r(H_2)$ value obtained over 2 h, indicating that H_2/O_2 recombination does not contribute significantly to the overall reaction during this time period.

For better comparison of the efficiency of the different redox catalysts employed, we have replotted in Figure 6 the hydrogen evolution rates, obtained from the three systems investigated, as a function of wavelength domain of excitation. A trend which

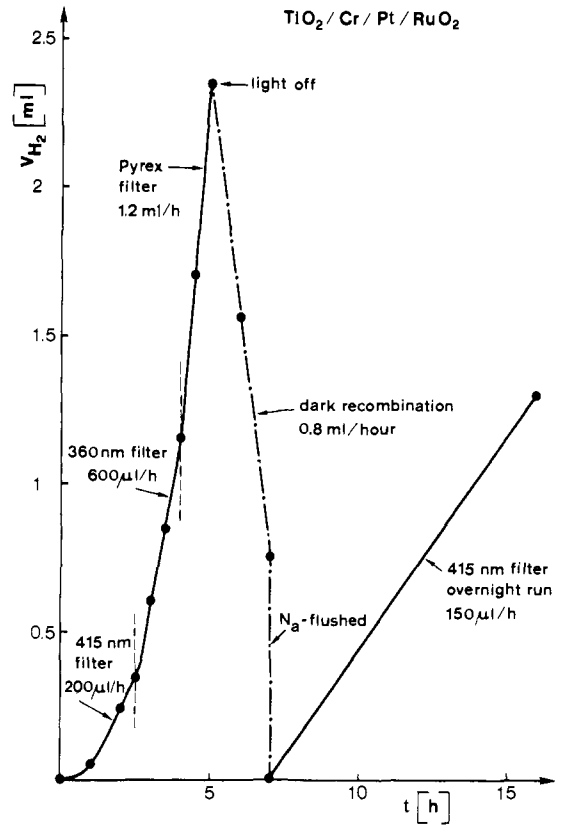

Figure 5. Light-induced water cleavage in TiO_2/Cr dispersions (Cr doping 570 ppm, annealed at 400 °C) loaded with 1% Pt and 0.2% RuO_2. Conditions as in Figures 3 and 4.

is generally obeyed is that the photoactivity of the TiO_2/Cr particles increases drastically upon loading with redox catalyst. The efficiency of the latter to mediate photoinduced H_2O decomposition increases in the order $RuO_2 < Pt \ll RuO_2/Pt$. Thus if visible light is used for excitation, Pt is twice as active as RuO_2.

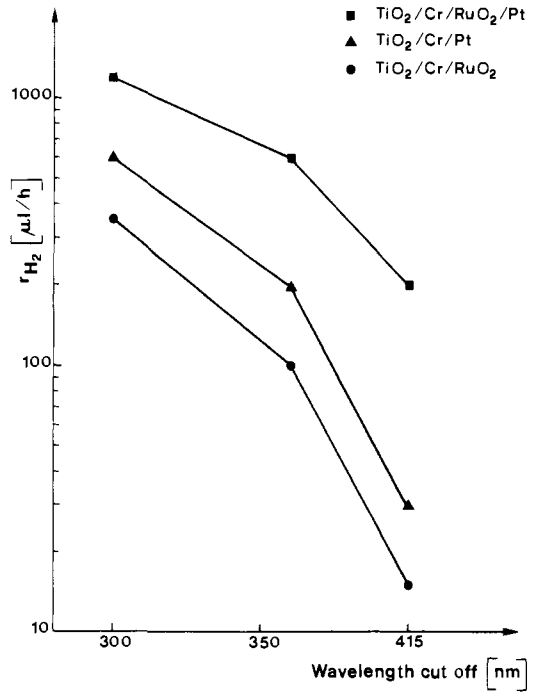

Figure 6. Comparison of hydrogen evolution rates for TiO_2/Cr particles loaded with Pt, RuO_2, or both redox catalyst. The abscissa indicates the lower wavelength limit of light used in the photolysis.

When both are codeposited onto the TiO_2/Cr carrier particle, the rate of hydrogen generation increases 7 to 13 times as compared to Pt or RuO_2 alone, respectively. Such a striking improvement, which by far exceeds the sum of the activities for the two individual components, implies that a synergistic effect is operative between the two redox catalysts. The quantum yield of visible light induced water cleavage ($\phi(H_2)$) achieved with such RuO_2/Pt-loaded TiO_2/Cr particles is only a factor of 6 smaller than that obtained with dye-sensitized semiconductor powders[13] and hence of the order of 1%.

To rationalize this behavior, we conceive the following mechanism for visible light induced water cleavage on TiO_2/Cr colloids: excitation of Cr^{3+} dopant, present mainly in the surface region of the particle, produces electrons in the conduction band of TiO_2 and holes, i.e., Cr^{4+}, which diffuse to the interface to afford hydrogen and oxygen formation from water, respectively. The former process is catalyzed by Pt sites while RuO_2 enhances hole transfer from Cr^{4+} to water resulting in oxygen generation. Selectivity of the redox catalysts in interacting with the two types of charge carriers may be provided by the type of junction formed between noble metal deposit and TiO_2/Cr support. Thus, Pt is likely to yield an ohmic contact while a Schottky barrier may be formed by RuO_2. This would direct the electron flow to the Pt sites while the holes would be trapped by RuO_2. Note that only a small barrier height, i.e., ~100 mV, is required to introduce such a selective interaction.[33]

The difference in photoactivity between Pt- and RuO_2-loaded colloids arises then from the kinetic characteristics for water reduction and oxidation on the TiO_2/Cr material, respectively. Hydrogen generation is strongly inhibited on single-crystal TiO_2 electrodes, and similar behavior is expected for our TiO_2/Cr particles. The ultrafine Pt deposit facilitates the cathodic process by greatly reducing the overvoltage requirement for H_2 formation. As for water oxidation by photogenerated minority carriers, one infers from results obtained with $SrTiO_3$ electrodes[34] that this reaction is also relatively slow. The role of RuO_2 is to accelerate this hole transfer process. Nevertheless, from the fact that $TiO_2/Cr/Pt$ particles produce twice as much H_2 as those loaded with RuO_2, it appears that the presence of a catalyst mediating the cathodic reaction is more beneficial for water decomposition than that involved in the anodic part. One concludes that the kinetic inhibition for H_2 generation by conduction-band electrons is more severe than that for the complementary hole reaction, i.e., O_2 formation from water and Cr^{4+}.

The argument may be brought forward that RuO_2 and Pt cannot interact selectively with holes and electrons and, in fact, catalyze both the water reduction process, water oxidation being fast even in the absence of catalyst. The higher $r(H_2)$ value obtained with Pt as compared to RuO_2 loaded particles could simply reflect the better electrocatalytic properties of the former material. However, such a mechanism is refuted by the findings obtained with TiO_2/Cr particles loaded simultaneously with Pt and RuO_2. If both catalysts would intervene in the same electrochemical process, one would expect their efficiency to be additive.[35] Furthermore, increasing the loading of one component should produce the same effect as adding the other. None of these predictions could be verified experimentally. In fact, from Figure 5 it is apparent that the activity of the bifunctional redox catalyst is about 1 order of magnitude higher than that obtained with the individual components. Such a synergistic effect can only be explained by the specific and combined intervention of highly dispersed Pt and RuO_2 in the cathodic and anodic events leading to visible light induced water decomposition.

Returning to Figure 6, one notices a significant increase in the rate of photoinduced water cleavage when the onset length of excitation is shifted from 415 to 300 nm. Thus $r(H_2)$ is 23, 20, and 8 times higher for RuO_2-, Pt-, and RuO_2/Pt-loaded TiO_2/Cr particles, respectively, if UV ($\lambda > 300$ nm) instead of visible light is used for photolysis. This augmentation is attributed to direct band-gap excitation of the TiO_2 support by UV light. Interestingly, when Pt/RuO_2-loaded TiO_2 particles that did not contain any Cr^{3+} were irradiated with UV light, the hydrogen output is practically the same as that obtained with Cr^{3+}-doped samples. This finding contrasts with the effects observed with TiO_2 or $SrTiO_3$ electrodes where Cr^{3+} doping reduces significantly the optical to current conversion efficiency for band-gap irradiation. The difference is attributed to the minute size of our semiconductor particles, which ensures that practically all the minority charge carriers reach the interface before recombination with electrons can occur. Another important result obtained with undoped $Pt/RuO_2/TiO_2$ particles is that they are inactive for water decomposition with visible light. No hydrogen formation is perceptible when these suspensions are illuminated through a 400-nm cutoff filter. This shows unambiguously that Cr^{3+} excitation is the origin of visible light induced water decomposition with chromium-doped TiO_2.

A further effect apparent from Figure 6 is that the difference in photoactivity obtained with the three catalysts is smaller in the UV than in the visible. Thus $r(H_2)$ increases only 4 times when TiO_2 loaded with both RuO_2 and Pt instead of TiO_2/RuO_2 is irradiated with $\lambda > 300$-nm light. A plausible explanation for this finding is that due to the higher rates of water decomposition, H_2 and O_2 accumulate more rapidly under UV than under visible-light irradiation, and hence, the back reaction between H_2 and O_2 can no longer be neglected. Therefore, the hydrogen formation rate of 1.2 mL/h found for the Pt/RuO_2-loaded TiO_2 particles represents only a lower limit for the true water decomposition rate. From Figure 5 one derives for the latter a value of $r(H_2) = 2$ mL/h if the recombination of H_2 and O_2 is taken into account.

Kinetics of Light-Induced Oxygen Generation. An example for oxygen evolution kinetics, typical for water-cleavage experiments in closed systems, is shown in Figure 7. The amount of O_2 produced from irradiating 25 mg of TiO_2/Cr loaded with both Pt and RuO_2 and dispersed in 25 mL of water (pH 3, adjusted with HCl) is plotted as a function of irradiation time. The experiment was started with no filter in the light beam. Very little

(33) Recently it was shown that a Schottky barrier is formed at the CdS/RuO_2 interface (Gissler, W.; Mc.Evoy, A. J.; Grätzel, M. *J. Electrochem. Soc.*, in press).

(34) Van den Kerchove, F.; Vandermden, J.; Gomes, W. P.; Cardon, F. *Ber. Bunsenges. Phys. Chem.* **1979**, *83*, 230.

(35) The low loading with Pt and RuO_2 makes the formation of RuO_2/Pt mixtures on the surface very unlikely.

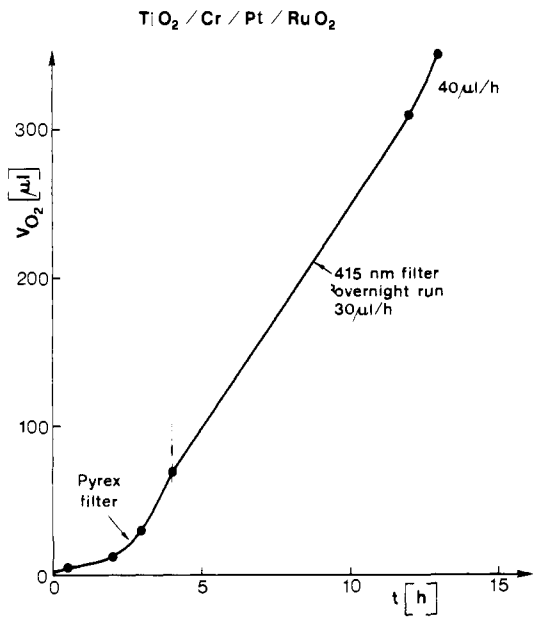

Figure 7. Kinetics of light-induced oxygen generation from water in the cyclic water decomposition systems. Conditions as in Figure 5.

O_2 is detectable in the gas phase initially. After 3 h of irradiation, the value of $r(O_2)$ was 50 μL/h. Since the initial rate of hydrogen generation measured simultaneously was 1.2 mL/h, this accounts for only ca. 8% of the stoichiometric value. A 400-nm filter was then inserted in the light beam and an overnight run with visible wavelength excitation performed, which yielded an average of $r(O_2) = 30$ μL/h and $r(H_2) = 150$ μL/h; i.e., $r(O_2)/r(H_2) = 0.2$. The actual rate of O_2 generation had, however, already increased to 40 μL/h ($r(O_2)/r(H_2) \simeq 0.3$) (after this irradiation time) and was found to augment further under prolonged illumination, $r(O_2)$ values obtained exceeding 80% of the stoichiometrically expected value.

The fact that oxygen does not appear initially in the gas phase arises from photoinduced uptake of O_2 by the TiO_2 support material. Munuera[36] has found that this process occurs most efficiently on highly hydroxylated anatase, i.e., the same material employed in our experiments. Chemisorption of O_2 onto the TiO_2 surface occurs via reduction by conduction-band electrons producing $HO_2\cdot$ radicals.[37]

The kinetics of photoinduced oxygen uptake by our TiO_2 samples were examined in aqueous dispersions of $TiO_2/RuO_2/Pt$ (12.5 mg/25 mL). Loading with catalyst was the same as in the foregoing experiments. The microfuel system was used for O_2 detection. The solution was first deaerated with N_2; the flask was then closed and after injection of 1 mL of O_2 subjected to UV radiation. After a given time period the photolysis was interrupted. Residual O_2 present in the flask was flushed out with N_2 and transferred to the microfuel cell, where it was quantatively analyzed. (The photoadsorbed fraction of O_2 corresponds to the differences between initially injected and residual oxygen.) Photouptake of O_2 was found to occur rapidly, 0.5 mL being adsorbed in ca. 20 min. After illuminating for 1 h, the amount of oxygen decreased to 20% of its initial value. Repeating the injection of 1 mL of O_2 leads again to photoadsorption. However, saturation of the TiO_2 is found after 3-4 injections, where the system approaches its limiting capacity for O_2 uptake and no more oxygen is photoadsorbed.

Similar results are obtained with TiO_2 dispersions that produce oxygen in situ under illumination. For example, exposure of dispersions of TiO_2/Cr (25 mg/25 mL) loaded with 0.2% RuO_2 to visible light in the presence of $AgNO_3$ (5×10^{-2}M, pH 4.5) leads to generation of oxygen. However, no H_2 is evolved as the conduction-band electrons produced by Cr^{3+} excitation reduce Ag^+ to elemental silver, which is deposited onto the TiO_2 particles.[38]

$$Ag^+ + e^-(CB) \rightarrow Ag \quad (1)$$

The decrease in silver ion concentration during photolysis was followed by using a Ag^+ specific electrode. In a typical experiment, 45 μL of O_2, i.e., 2×10^{-6} mol, is produced after 1 h of irradiation, while the decrease in silver ions amounts to 8×10^{-5} M. This accounts for only 10% of the stoichiometrically expected quantity of O_2. This parallels the results obtained in the water-cleavage experiments where the amount of initially detectable oxygen was also far below the stoichiometric value. In both cases the main part of O_2 produced is withheld at the surface of the TiO_2 particle. We found that the adsorbed fraction can be released by adding sodium phosphate to the TiO_2 dispersion. In the experiment described above, 40 μL of O_2 was obtained after 1 h of visible-light photolysis of $TiO_2/Cr/RuO_2$ dispersions in aqueous $AgNO_3$. Subsequently 3% Na_3PO_4 was added and the mixture stirred in the dark under nitrogen for 3-4 h. During this period, an additional 200 μL of O_2 was desorbed from the TiO_2 particles as shown by microfuel technique analysis. The total amount of oxygen accounts for 75% of the reduced Ag^+ ions.

Similar results were obtained with TiO_2/Cr dispersions used for the visible light induced water cleavage experiments described in the previous section. Solutions treated with Na_3PO_4 after illumination were found to release oxygen. If, on the other hand, Na_3PO_4 is added prior to photolysis, photouptake of O_2 is prevented, and hydrogen and oxygen are cogenerated in approximately stoichiometric proportion.[39] However, the quantum yield of ater cleavage is here much smaller than in phosphate-free solutions.

It is also possible to increase the rate of oxygen generation by adding electrolyte to the dispersion prior to illumination. These results are summarized in Table I for two acceptors, i.e., Ag^+ and Fe^{3+}. In the case of $AgNO_3$, the rate of oxygen generation increases from 40 μL/h to 80 μL/h upon addition of 5×10^{-2} M Na_2SO_4. If Fe^{3+} is used as an electron acceptor, addition of 10^{-3} M Li_2CO_3 triples the $r(O_2)$ value from 15 to 45 μL/h. These effects indicate that the presence of ions strongly affects the photoadsorption of O_2 to the surface of TiO_2 particles as was noted earlier by Munuera et al.[36]

A final effect investigated concerns the influence of RuO_2 on the oxygen generation rate. Using the same conditions as outlined in Table I for the $AgNO_3$ system without Na_2SO_4, we obtained $r(O_2) = 30$ and 45 μL/h for TiO_2/Cr particles without, and loaded with, 0.5% RuO_2, respectively. This distinctive acceleration of water oxidation induced by the RuO_2 deposit lends strong support to our earlier contention that the latter intervenes as a selective hole-transfer catalyst in the water decomposition by visible light.

Table I. Effect of Electrolyte on the Visible Light ($\lambda > 415$ nm) Induced O_2 Generation with TiO_2/Cr Dispersions in the Presence of Acceptors

acceptor	additive	TiO_2, μL/h
$AgNO_3$ (5×10^{-2} M), pH 3.5	none	40
	5×10^{-2} M Na_2SO_4	80
$Fe_2(SO_4)_3$ ($[Fe^{3+}] = 5 \times 10^{-2}$ M, pH 1.6	none	15
	1×10^{-3} M Li_2CO_3	45

Conclusions

The present study shows for the first time that visible light induced water cleavage can be achieved with transition metal ion doped TiO_2 particles. This constitutes a distinctive progress with respect to earlier TiO_2 or $SrTiO_3$ based systems[26,40] where UV

(36) Munuera, G.; Rives-Arnau, V.; Sancedo, A. *J. Chem. Soc., Faraday Trans. 1* **1979**, 736.
(37) Jaeger, C. D.; Bard, A. J. *J. Phys. Chem.* **1979**, *24*, 3146.
(38) Kraeutler, B.; Bard, A. J. *J. Am. Chem. Soc.* **1978**, *100*, 4317 and references cited therein.
(39) Phosphate ions show a strong affinity for adsorption to TiO_2 and therefore compete with oxygen for surface sites. (Boehm, H. P. *Faraday Discuss. Chem. Soc.* **1971**, *52*, 364.)

light was required to afford water decomposition. With respect to Cr^{3+}-doped TiO_2 electrodes, the colloidal semiconductor particles have the advantage that the small minority carrier diffusion length does not decrease the quantum yield of H_2 formation from band-gap excitation. The use of very small semiconductor particles was combined here with the concept of electrocatalysis for water reduction and oxidation by ultrafine noble metal deposits. A striking synergistic effect was shown to be operative between RuO_2 and Pt, underlining again the superiority of this catalyst combination in water photolysis systems.

Important information has also been obtained on the role of the TiO_2 support material as an oxygen carrier. Photouptake of O_2 by our hydroxylated anatase decreases the concentration of free oxygen in solution, which allows light-induced water cleavage to proceed at a high yield. The buildup of O_2 is a key problem in all devices that attempt to cogenerate H_2 and O_2 without local separation, since the latter competes with protons for reduction on Pt sites. Further studies will therefore be directed to increase the capacity for O_2 uptake of the system. Through introduction of supplementary heterogeneous oxygen carriers, it should be possible to develop systems that under solar irradiation will produce pure hydrogen, oxygen being retained on a carrier that releases it during the night.

Acknowledgment. This work was supported by the Swiss National Science Foundation and in part by CIBA Geigy, Basel. E.P. thanks the CNR, Italy, for support.

Registry No. TiO_2, 13463-67-7; RuO_2, 12036-10-1; Cr^{3+}, 16065-83-1; Pt, 7440-06-4; H_2O, 7732-18-5.

(40) (a) Bulatov, A. V.; Khidekel, M. L. *Izv. Akad. Nauk SSSR, Ser. Khim.* **1976**, 1902. (b) Schrauzer, G. N.; Guth, T. D. *J. Am. Chem. Soc.* **1977**, *99*, 7189. (c) van Damme, H.; Hall, W. K. *Ibid.* **1979**, *101*, 4373. (d) Sato, S.; White, J. M. *Chem. Phys. Lett.* **1980**, *72*, 83. (e) Kawai, T.; Sakata, T. *Ibid.* **1980**, *72*, 87. (f) Domen, K.; Naito, S.; Sorna, M.; Onishi, T.; Tamuru, K. *J. Chem. Soc., Chem. Commun.* **1980**, 543. (g) Kawai, T.; Sakata, T. *Nature (London)* **1980**, *286*, 474. (h) Wagner, F. T.; Somorjai, G. A. *Ibid.* **1980**, *285*, 559. (i) Lehn, J. M.; Sauvage, J. P.; Ziessel, R. *Nouv. J. Chim.* **1980**, *4*, 623. (j) Sato, S.; White, J. M. *J Catal.* **1981**, *69*, 128.

Ground- and Excited-State Conformational Differences between Diastereomeric Dipeptides

Chieu D. Tran, Godfrey S. Beddard, Rose McConnell, Charles F. Hoyng, and Janos H. Fendler*

Contribution from the Department of Chemistry, Texas A&M University, College Station, Texas 77843. *Received October 20, 1980*

Abstract: Ground- and excited-state conformations of D-tryptophanyl-L-tryptophan methyl ester ($\mathbf{1}_{DL}$) L-tryptophanyl-L-tryptophan methyl ester ($\mathbf{1}_{LL}$) have been investigated by ^1H NMR and by steady-state and subnanosecond time-resolved fluorescence lifetime and anisotropy measurements. Examination of ^1H NMR spectra of cyclic L-tryptophanyl-L-tryptophan and of $\mathbf{1}_{DL}$ and $\mathbf{1}_{LL}$ at different temperatures suggested that the two indole rings are close to each other in $\mathbf{1}_{DL}$ but not in $\mathbf{1}_{LL}$. Flourescence decays of $\mathbf{1}_{DL}$ and $\mathbf{1}_{LL}$ in Me_2SO and MeOH and in glycerol–methanol mixtures have been fitted to $I(t) = A[fe^{-t/\tau_1} + (1-f)e^{-t/\tau_2}] + B$, where τ_1 and τ_2 are fluorescence decay times, A is the amplitude, and B is the background. Differences in the mean decay times, τ_m ($\tau_m = f\tau_1 + (1-f)\tau_2$), between $\mathbf{1}_{DL}$ and $\mathbf{1}_{LL}$ reflected different degrees of quenching of the chromophores due to different conformations. No diastereomeric selectivity has been observed, however, in the quenching of τ_m by CCl_4. Plots of rotational correlation times, τ_R values, against solvent viscosities for $\mathbf{1}_{DL}$ and $\mathbf{1}_{LL}$ gave slopes of 21.2 and 17.1 ps/cP, respectively. These values are larger than those expected from the Stokes–Einstein equation, assuming the stick boundary conditions. The observed τ_R values for **1** have been discussed in terms of four possible behaviors related to rapid or fixed motions of the two tryptophans and to the fast and slow energy transfers between the two indole moieties during the excited-state lifetime as well as in terms of long-lived volume fluctuations of the solvent.

Differences in chemical and physical properties of diastereomers have been the subject of much theoretical[1,2] and experimental[3-5] studies. Diastereomeric differences in dipeptides are particularly important since protein folding is affected by side-chain conformations.[6,7] Ground- and excited-state conformations of D-tryptophanyl-L-tryptophan methyl ester ($\mathbf{1}_{DL}$) and L-tryptophanyl-L-tryptophan methyl ester ($\mathbf{1}_{LL}$) have been investigated in the present work, therefore, by ^1H NMR and by steady-state and subnanosecond time-resolved fluorescence anisotropy. Introducing an indole moiety into the dipeptides enhances the differences in chemical shifts between the diastereomers.[8] Methyl esters were chosen to alleviate problems associated with protein transfer.[9] Ground-state conformational differences between diastereomeric **1** have been investigated by ^1H NMR spectroscopy. The importance of intrinsic fluorescence of tryptophan residues in proteins[10-12] has prompted us to place greater emphasis on subnanosecond time resolved fluorescence spectroscopy which provided information on exicted-state conformations of these dipeptides.

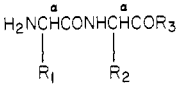

1, R_1 = $C^\beta H_2$-indole, R_2 = $C^\beta H_2$-indole, R_3 = OMe
$\mathbf{1}_{LL}$, L-Trp-L-Trp-OMe
$\mathbf{1}_{DL}$, D-Trp-L-Trp-OMe
$\mathbf{1}_{DD}$, D-Trp-D-Trp-OMe
$\mathbf{1}_{LD}$, L-Trp-D-Trp-OMe
2, R_1 = CH_2-indole, R_2 = CH_3, R_3 = OH (L-Trp-L-Ala-OH)
3, R_1 = CH_3, R_2 = CH_2-indole, R_3 = OH (L-Ala-L-Trp-OH)

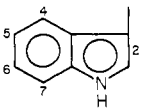

indole

The obtained results have been rationalized in terms of a folded structure for $\mathbf{1}_{DL}$ in which the two indole rings are approximately

*To whom correspondence should be address at Clarkson College of Technology, Potsdam, NY 13676.

(1) Craig, D. P.; Mellor, D. P. *Fortschr. Chem. Forsch.*, **1976**, *63*, 1.

0002-7863/82/1504-3002$01.25/0